



# High-temperature viscosity of many-component glass melts



Pavel Hrma<sup>a,\*</sup>, Albert A. Kruger<sup>b</sup>

<sup>a</sup> Pacific Northwest National Laboratory, Richland, WA 99354, United States

<sup>b</sup> U.S. Department of Energy, Office of River Protection, Richland, WA 99352, United States

## ARTICLE INFO

### Article history:

Received 12 November 2015

Received in revised form 5 January 2016

Accepted 15 January 2016

Available online xxxx

### Keywords:

Glass-melt viscosity

Glass melting

Nuclear waste glass

Viscosity models

## ABSTRACT

In this article, we argue that 1) the activation energy for viscous flow becomes independent of temperature when the viscosity of molten glass is sufficiently low at high enough temperatures, such as those that exist in a glass-melting furnace, and 2) the intercept of the linear function  $\ln\eta$  versus  $T^{-1}$  ( $\eta$  is the viscosity and  $T$  is the temperature) is independent of glass composition. This hypothesis, which is hardly new and is well supported by experimental data, allows minimization of the number of fitting parameters. A new dataset of meticulously measured viscosities of a large composition region of simulated nuclear waste glasses that recently became available provided an excellent opportunity to test this hypothesis to verify it again. Also, we used this dataset to demonstrate that some popular functions designed for representing the high-viscosity segment (where the activation energy changes with temperature) are not recommendable for approximating the low-viscosity segment (where the activation energy is constant). Fitting such functions produces overparameterization and leads to physically meaningless (or at least esthetically unsatisfactory) outcomes, or, if the functions are constrained by the glass-transition viscosity and the high-temperature asymptote, the result is a significant lack of fit.

© 2016 Elsevier B.V. All rights reserved.

## 1. Introduction

Establishing approximation functions for property-composition relationships (also called models) requires a sufficient number of reliable data. Generally, large databases may cover the multidimensional composition regions more densely (though not necessarily more uniformly than the small ones), thus allowing for identifications of secondary effects, such as component interactions. A previous paper [1] analyzed a low-viscosity database containing nearly 7000 data points from over 1300 glass compositions. The database was made available in 2009 and contained data accumulated from several laboratories over several years. Such a large database has an advantage in the large volume of information, but its drawback is that it can contain hidden parameters associated with different methods of measurement in different laboratories by researchers with different levels of training using different chemicals, different glass preparation procedures, etc. This diversity increases the uncertainty of the models and the number of outlying data can be large. The different test conditions introduce additional sources of uncertainty in measured quantities. Consequently, model coefficients and model predictions associated with models developed using these measured quantities can have greater uncertainty than they would have if the hidden parameters were not present in the dataset.

Smaller, well-designed datasets can be free of the uncertainties of large data collections. In another work [2], a test matrix was designed for 38 glass compositions by changing one component at a time, starting

from a centroid composition, from which component fractions were varied in regular intervals. Temperatures were also varied by regular increments. The dataset contained 323 viscosity values. Viscosity measurements were performed using a strict procedure, which was followed meticulously. Data analysis revealed slightly nonlinear behavior with respect to composition that nevertheless allowed a linear (first-order) model to be fitted with a high precision ( $R^2 = 0.993$ ).

This paper uses a dataset reported by the Vitreous State Laboratory (VSL) [3]. The dataset was produced using a strictly controlled procedure, thus being free of uncontrolled influences, but has not been designed specifically for modeling viscosity versus composition. The glass compositions were formulated for melter experiments aimed at testing glasses for potential applications in the Hanford Waste Treatment and Immobilization Plant, which is under construction, to process a limited number of high-level nuclear wastes anticipated for vitrification [3]. Compositions were varied by changing waste loading and fractions of additive components to achieve glasses with acceptable properties and behavior in melters of various scales. Naturally, some waste component fractions were linearly dependent to some extent and fractions of the major components, though free of unacceptable collinearities, were not evenly distributed over their respective ranges, leaving gaps in the composition region coverage.

The main purpose of this study is to determine the minimum number of parameters and corresponding model form needed to represent the high-temperature viscosity as a function of temperature and melt composition. The VSL dataset was chosen for this study because the composition region covered by the VSL dataset is larger than any composition region previously tested (see Table 1) and is the focus for

\* Corresponding author.

E-mail address: [pavel.hrma@pnnl.gov](mailto:pavel.hrma@pnnl.gov) (P. Hrma).

**Table 1**

Average, maximum, and minimum component mass fractions ( $g_{ai}$ ,  $g_{Mi}$ , and  $g_{mi}$ ) for the 26-component (including “Others”) dataset.

	$g_{ai}$	$g_{Mi}$	$g_{mi}$
SiO <sub>2</sub>	0.3718	0.5310	0.1944
Al <sub>2</sub> O <sub>3</sub>	0.1344	0.2664	0.0193
B <sub>2</sub> O <sub>3</sub>	0.1334	0.2021	0.0430
Na <sub>2</sub> O	0.1135	0.2000	0.0358
Fe <sub>2</sub> O <sub>3</sub>	0.0890	0.2001	0.0268
Li <sub>2</sub> O	0.0289	0.0575	0
CaO	0.0244	0.1820	0.0023
P <sub>2</sub> O <sub>5</sub>	0.0135	0.0548	0
Bi <sub>2</sub> O <sub>3</sub>	0.0133	0.0738	0
MnO	0.0119	0.0800	0
ZrO <sub>2</sub>	0.0117	0.1064	0.0004
K <sub>2</sub> O	0.0095	0.0767	0
ZnO	0.0061	0.0400	0
Others	0.0061	0.0160	0.0001
NiO	0.0051	0.0212	0
Cr <sub>2</sub> O <sub>3</sub>	0.0044	0.0300	0.0006
MgO	0.0042	0.0312	0
UO <sub>3</sub>	0.0036	0.0556	0
F	0.0033	0.0097	0
SrO	0.0030	0.0927	0
PbO	0.0025	0.0321	0
TiO <sub>2</sub>	0.0020	0.0162	0
ThO <sub>2</sub>	0.0015	0.0360	0
La <sub>2</sub> O <sub>3</sub>	0.0012	0.0120	0
CdO	0.0008	0.0085	0
V <sub>2</sub> O <sub>5</sub>	0.0006	0.0250	0

melter application. Only low-viscosity data were collected for melts processed in the waste-glass melters. Viscosities ranged from 0.4 to 462 Pa s (17 Pa s average), and the temperatures ranged from 941 to 1315 °C (1120 °C average).

## 2. Approximation function

The viscosity of molten glass is affected by every component present in a sufficient concentration. Therefore, the viscosity of many-component glasses, such as geological glasses or nuclear waste glasses, is a function of a large number of compositional variables. Nuclear waste glasses tend to contain 40 to 60 components. In such “crowded” mixtures, the large number of components imposes limits on the ranges of component fractions. Its composition region is large in terms of dimensions in the composition space, but small in terms of the intervals of composition variables. For such a region, nonlinear effects are relatively minor and component interactions can be disregarded unless they are caused by microstructural phenomena preceding crystallization or phase separation.

Viscosity is a strong function of temperature; the relationship is affected by structural changes that molten glass undergoes in response to changing temperature. As temperature increases, glass becomes progressively “depolymerized” until, at a low enough viscosity (the value of which depends on glass fragility), the melt begins to behave like an ordinary simple liquid. For fragile glasses, such as nuclear waste glasses, this happens at a viscosity lower than 100 Pa s. In the glass-melting furnaces, the viscosity is never higher than 100 Pa s. This paper is solely focused on the low-viscosity region.

Because the activation energy ceases to be temperature dependent for low-viscosity melts, a simple Arrhenius-type function is appropriate as an approximation function:

$$\ln \eta = A + \frac{B}{T} \quad (1)$$

where  $\eta$  is the viscosity,  $T$  is the temperature,  $A$  is a constant, and  $B$  is the activation energy (in K). The pre-exponential factor,  $\eta_\infty = e^A$ , is independent of composition, at least for a family of glasses of a similar

strength (in terms of fragility). The activation energy depends on composition and can be expressed, at first approximation, as the first-order polynomial in terms of mass (or mole) fractions of components:

$$B = \sum_{i=1}^N B_i g_i \quad (2)$$

where  $B_i$  is the  $i$ -th component coefficient and  $g_i$  is the  $i$ -th component mass fraction. Mole fractions can also be used, and would be favored by researchers oriented toward the atomic structures of melts, but here we prefer mass fractions for practical purposes: glasses are prepared by weighing the raw materials. When fitting Eqs. (1) and (2) to viscosity data, the fitting parameters are the  $N$  values of  $B_i$  coefficients and a single value of  $A$ . Hence, the number of fitting parameters is  $p = N + 1$ . See Section 6 for possible extension of Eq. (2) to include secondary effects.

The  $B_i$  coefficients are partial specific activation energies for viscosity (partial molar activation energies in the case of mole fractions). Consequently, the  $B_i$ s are properties of the melt structure and are constant when the viscosity is low enough that the melt structure is not significantly affected by increasing temperature.

The viscosity dataset consists of viscosity-temperature data pairs for a variety of glass compositions. To obtain  $A$  and  $B_i$  values, the combined Eqs. (1) and (2) are fitted to data using regression via minimizing the value of data deviation,  $D_\eta$ :

$$D_\eta = \sum_{j=1}^n \left( \ln \eta_{Mj} - A - \frac{B_{Ej}}{T_j} \right)^2 = \sum_{j=1}^n \left( \ln \frac{\eta_{Mj}}{\eta_{Ej}} \right)^2 \quad (3)$$

where  $n$  is the number of data points, the subscripts  $M$  and  $E$  denote the measured and model-estimated value, respectively, and the subscript  $j$  stands for the  $j$ -th data point. It is also possible to use a fixed value of  $A$  (if  $A$  is a known constant for a specific family of glasses) and use linear regression to minimize the value of

$$D_B = \sum_{j=1}^n [T_j (-A + \ln \eta_{Mj}) - B_{Ej}]^2 = \sum_{j=1}^n (B_{Mj} - B_{Ej})^2 \quad (4)$$

## 3. Viscosity dataset

The VSL high-level waste (HLW) glass property dataset [3] lists 276 glass compositions; for 101 of these, there are altogether 400 viscosity-temperature pairs measured at 2 to 5 temperature values for each glass. Of the staggering number of 57 components (oxides of 55 elements plus 2 halogens), only 25 were present at a fraction higher than 0.75 mass% in the viscosity subset. The fractions of components of less than 0.75 mass% were summed into an “Others” component (0.01–1.60 mass%, 0.61 mass% average). Table 1 lists the average ( $g_{ai}$ ), maximum ( $g_{Mi}$ ), and minimum ( $g_{mi}$ ) component mass fractions. Note that the minimum mass fraction of all but 8 components (SiO<sub>2</sub>, B<sub>2</sub>O<sub>3</sub>, Na<sub>2</sub>O, Fe<sub>2</sub>O<sub>3</sub>, Al<sub>2</sub>O<sub>3</sub>, CaO, Cr<sub>2</sub>O<sub>3</sub>, and ZrO<sub>2</sub>) was zero.

Eqs. (1) and (2) were combined and the resulting equation was initially fitted to the 25-component dataset plus “Others” to obtain estimates for both the  $A$  and the set of first-order polynomial coefficients,  $B_i$ . Some minor waste components exhibited unlikely large or small  $B_i$  values. Several minor oxides, Cr<sub>2</sub>O<sub>3</sub>, NiO, MnO, and ZnO, tend to form spinel with Fe<sub>2</sub>O<sub>3</sub>, and P<sub>2</sub>O<sub>5</sub> tends to form calcium phosphate crystals that may nucleate from phase-separated droplets. In addition, some waste components were codependent to an unacceptable degree: the Pearson’s correlation coefficient for NiO versus P<sub>2</sub>O<sub>5</sub> was 0.81. To avoid inaccurate values of component coefficients from the regression analysis, the troublesome components were added to “Others” together with the minor uninformative components (V<sub>2</sub>O<sub>5</sub>, CdO, TiO<sub>2</sub>, ThO<sub>2</sub>, UO<sub>3</sub>, La<sub>2</sub>O<sub>3</sub>, and PbO). The remaining 14 components (Al<sub>2</sub>O<sub>3</sub>, B<sub>2</sub>O<sub>3</sub>, Bi<sub>2</sub>O<sub>3</sub>,

CaO, F, Fe<sub>2</sub>O<sub>3</sub>, K<sub>2</sub>O, Li<sub>2</sub>O, MgO, MnO, Na<sub>2</sub>O, SiO<sub>2</sub>, SrO, and ZrO<sub>2</sub>) were selected for further analysis. For the “Others” component, the maximum mass fraction increased to 0.146, minimum to 0.019, and average to 0.047.

**4. Arrhenius model**

Table 2 presents *B<sub>i</sub>* coefficients (in 10<sup>4</sup> K) and some basic statistics for a model with *N* = 15 components (including “Others”). After excluding a high-viscosity outlier, 462 Pa s at 974 °C, out of the original 400 (*η*, *T*) pairs, initial optimization was performed for *n* = 399 (*η*, *T*) pairs. The final optimization was done for *n* = 395 (*η*, *T*) pairs, excluding 4 additional data with *D<sub>η</sub>* = [ln(*η<sub>M</sub>*/*η<sub>E</sub>*)]<sup>2</sup> > 0.3 or *D<sub>B</sub>* = (*B<sub>M</sub>* − *B<sub>E</sub>*)<sup>2</sup> > 0.01. Both *A* and *B<sub>i</sub>* values were estimated using Eq. (3). The resulting *A* value was then used in Eq. (4) to obtain the second set of *B<sub>i</sub>* coefficients and their standard errors.

Note the high values of standard errors (StEr) of the *B<sub>i</sub>* coefficient for F, a volatile component present in a small fraction of <1 mass%; F was included in the influential component set because it has a strong ability to decrease melt viscosity [4,5]. The high StEr of *B<sub>i</sub>* for F was likely associated with its low fraction in glasses rather than with its volatility. According to the 2009 database [6], up to 0.06 mass% F was added to 926 glasses, of which 287 were analyzed, finding 43 to 120% F (94% average) of the nominal (batched) value; F was also found as an impurity in 50 glasses, to which it was not added as a component. Hence, the large database [6] provides little evidence for F losses from melts with low F concentrations.

Based on the final optimization, the values of *B* varied for individual glasses on the dataset from the *B<sub>m</sub>* = 1.54 × 10<sup>4</sup> K to *B<sub>M</sub>* = 2.03 × 10<sup>4</sup> K, where the subscripts *m* and *M* denote the minimum and maximum value, respectively. The average *B* was 1.83 × 10<sup>4</sup> K. Adding a component with *B<sub>i</sub>* > *B<sub>M</sub>* to the glass, while keeping fractions of other components in constant proportions, tends to increase viscosity of any glass within the composition region of model validity. Accordingly, only ZrO<sub>2</sub>, SiO<sub>2</sub>, and Al<sub>2</sub>O<sub>3</sub> tend to increase viscosity. Similarly, components with *B<sub>i</sub>* < *B<sub>m</sub>* tend to decrease viscosity within the composition region of model validity. These comprise all components other than ZrO<sub>2</sub>, SiO<sub>2</sub>, and Al<sub>2</sub>O<sub>3</sub>—most notably Li<sub>2</sub>O and Na<sub>2</sub>O—except MgO and “Others”, which have little effect. Accordingly, MgO tends to mildly decrease viscosity of glasses with *B* > *B<sub>MgO</sub>*, and vice versa. This is also true about “Others” as a whole, but obviously not about all “Others” individual components. Luckily, even though the *g<sub>i</sub>* values of “Others”

were rather high for most compositions, the overall effect of “Others” on viscosity remained insignificant.

Fig. 1 shows data deviation (*D<sub>η</sub>*) distribution for the original 400 viscosity-temperature data pairs. Large deviations indicate outliers (*D<sub>η</sub>* > 0.3). Note that estimated and measured values are almost identical for some data (*D<sub>η</sub>* < 1). The frequency of deviations, *f* = *dn*/*dz*, where *z* = ln(*η<sub>M</sub>*/*η<sub>E</sub>*) was normalized to the cumulative frequency ∫<sub>−∞</sub><sup>∞</sup> *f* *dz* = 1 and plotted against *z*. As the fitted bell curve indicates, the distribution is approximately Gaussian.

Removing outliers influenced neither the composition region nor the temperature span, but the maximum viscosity decreased from 462 Pa s (original dataset) to 242 Pa s (data selected for model fitting). Thus, the maximum *g<sub>i</sub>* values remained the same for the final dataset as for the original one listed in Table 1.

As Fig. 2 indicates, four outliers belonged to the lowest temperature group of data and one outlier belonged to the highest temperature group. Two outliers had the highest contents of both Al<sub>2</sub>O<sub>3</sub> (0.266) and CaO (0.182). The glass composition of the outlier with the highest viscosity (462 Pa s) did not have an extreme fraction of any major component and would have, based on the model, a viscosity 4 times lower (106 Pa s). This may be caused by network polymerization that sets in as temperature decreases (note that in this context, the term “polymerization” designates structural changes leading to an increase of *B* in response to decreasing temperature). Thus, the Arrhenius model does not apply to this data point. As Fig. 3 shows, the model underpredicts viscosity of data with the measured log(*η*/Pa s) > 2 (note that the component coefficients are defined in terms of the natural logarithm,

**Table 2**  
Values of 10<sup>−4</sup> *B<sub>i</sub>* (K) coefficients by regression analysis using Eqs. (3) and (4).

	Initial optimization			Final optimization		
	Eq. (3)	Eq. (4)	StEr	Eq. (3)	Eq. (4)	StEr
<i>n</i>	399	399	399	395	395	395
<i>A</i>	−11.384			−11.303		
Li <sub>2</sub> O	−4.428	−4.356	0.145	−4.356	−4.268	0.133
Na <sub>2</sub> O	−0.103	−0.079	0.108	−0.122	−0.060	0.099
CaO	0.260	0.239	0.114	0.139	0.175	0.106
F	0.391	0.192	1.096	0.816	0.642	1.005
B <sub>2</sub> O <sub>3</sub>	0.809	0.808	0.105	0.838	0.877	0.097
MnO	0.873	0.862	0.217	0.807	0.828	0.199
K <sub>2</sub> O	1.181	1.200	0.131	1.108	1.164	0.120
SrO	1.273	1.235	0.161	1.272	1.273	0.147
Bi <sub>2</sub> O <sub>3</sub>	1.390	1.376	0.213	1.360	1.375	0.196
Fe <sub>2</sub> O <sub>3</sub>	1.430	1.398	0.083	1.430	1.437	0.077
MgO	1.628	1.577	0.428	1.647	1.639	0.392
Others	1.963	1.949	0.085	1.932	1.936	0.078
ZrO <sub>2</sub>	2.649	2.576	0.169	2.624	2.589	0.155
SiO <sub>2</sub>	2.986	2.972	0.094	2.970	2.997	0.087
Al <sub>2</sub> O <sub>3</sub>	3.413	3.378	0.088	3.373	3.375	0.082
<i>R</i> <sup>2</sup>	0.9778	0.9265		0.9811	0.9378	
<i>R</i> <sup>2</sup> <sub>adj</sub>	0.9802	0.9238		0.9350	0.9355	
RMSE		0.0266			0.0244	

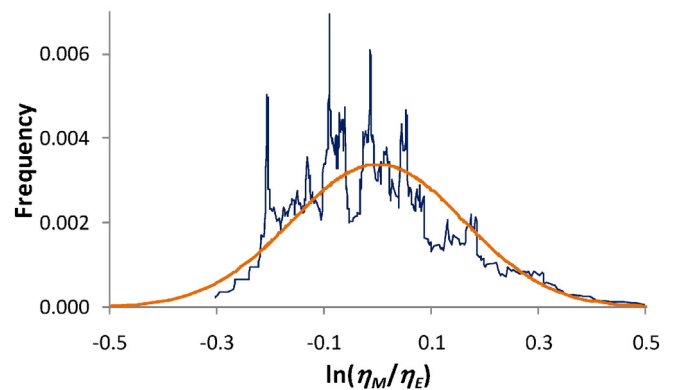
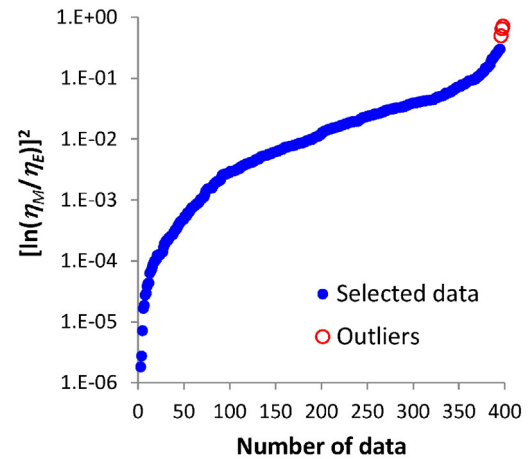


**Fig. 1.** Top: *D<sub>η</sub>* = [ln(*η<sub>M</sub>*/*η<sub>E</sub>*)]<sup>2</sup>, Eq. (3), versus *n* (data number sorted by *D<sub>η</sub>*). Empty circles indicate removed (outlying) data. Bottom: frequency, *f* = *dn*/*dz*, where *z* = ln(*η<sub>M</sub>*/*η<sub>E</sub>*) (normalized to the cumulative frequency ∫<sub>−∞</sub><sup>∞</sup> *f* *dz* = 1) versus *z*; the bell curve *f* = *f*<sub>0</sub>exp[−(*z*/*z*<sub>0</sub>)<sup>2</sup>] was fitted to data (*f*<sub>0</sub> = 0.00339 and *z*<sub>0</sub> = 0.226).

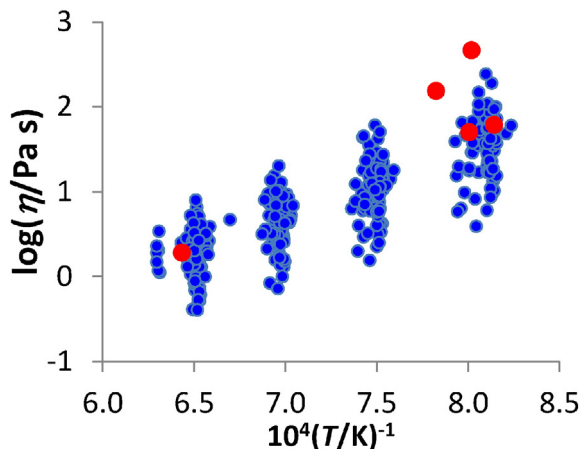


Fig. 2.  $\log \eta$  versus inverse temperature for the dataset of 400  $(\eta, T)$  pairs. Outliers are marked by large red circles. (For interpretation of the references to color in this figure legend, the reader is referred to the web version of this article.)

In  $\eta$ , while the decadic logarithm,  $\log \eta$ , is used when convenient for indicating the order of magnitude).

### 5. Model validation

Property-composition models are typically validated with data that are not included in the dataset to which the model equations were fitted but belong to the same or similar composition region. Thus, our model can be validated using viscosity data available for glasses designed for Hanford high-level wastes [6–10] or even glasses developed for Hanford low-activity wastes [11,12] or high-level wastes stored in other sites, such as Savannah River [13], as long as the pertinent composition regions sufficiently overlap. Historical data of commercial as well as waste glasses are plentiful and various models that represent them are available in the literature [14–17].

For validating the coefficients listed in Table 2 (those optimized with  $D_\eta$ , Eq. (3), using the VSL dataset of 395 data points), we selected previously reported statistically designed dataset [2] of 326  $(\eta, T)$  pairs and 13 components ( $\text{Al}_2\text{O}_3$ ,  $\text{B}_2\text{O}_3$ ,  $\text{Bi}_2\text{O}_3$ ,  $\text{CaO}$ ,  $\text{Fe}_2\text{O}_3$ ,  $\text{K}_2\text{O}$ ,  $\text{Li}_2\text{O}$ ,  $\text{MnO}$ ,  $\text{Na}_2\text{O}$ ,  $\text{P}_2\text{O}_5$ ,

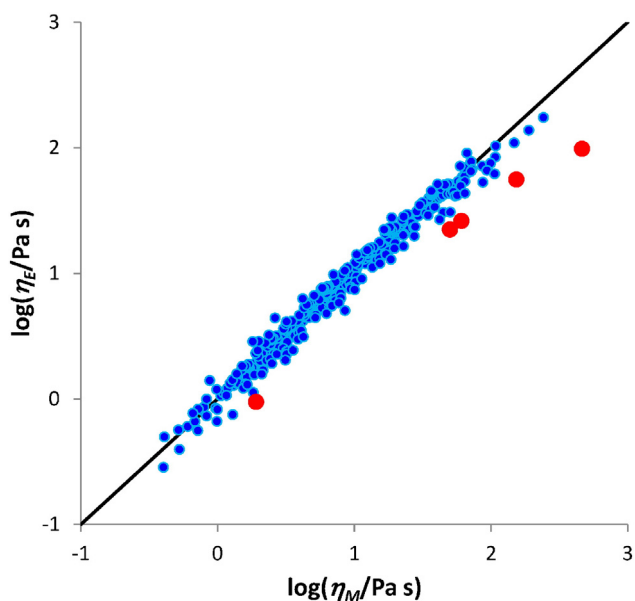


Fig. 3. Estimated versus measured values of  $\ln \eta$ . Outliers are marked by red circles. (For interpretation of the references to color in this figure legend, the reader is referred to the web version of this article.)

$\text{SiO}_2$ ,  $\text{ZrO}_2$ , and “Others”). The 15 components of the VSL data set and the 13 components of the validation dataset overlap in 12 components. To obtain estimated viscosity values for validation glasses (where F, MnO, and SrO are included in “Others”),  $\text{P}_2\text{O}_5$  was added to “Others”. Fig. 4 shows the result. The validation  $R^2$ , computed for  $\log \eta$ , was 0.9803. For all data,  $D_\eta = [\ln(\eta_M/\eta_E)]^2 < 0.2$ . The successful validation with a reliable dataset indicates that the drawbacks (with respect to model fitting) of the VSL dataset (gaps in composition region coverage and correlations in minor component fractions) did not negatively affect the model outcome.

Successful validation also indicates that the measured glass melt viscosity was not significantly affected by possible compositional nonuniformity or by volatilization and crystallization that occurred during glass preparation or viscosity measurement. The validation data were produced at the Pacific Northwest National Laboratory (PNNL) using different experimental procedures than the VSL used. Yet in both laboratories, a great care has been taken to prepare glasses as uniform in composition as possible. Whereas VSL homogenizes melts by mechanical stirring, PNNL is melting glasses twice: The first melt is prepared from batch chemicals; the glass is then ground and thoroughly homogenized before executing the second melt. Melting is performed in PtRh crucibles under PtRh lids. Both laboratories calibrate their viscometers, VSL with standard oils [3] and PNNL with standard glasses [7]. VSL routinely checks their compositions using the x-ray fluorescence method. A meticulous study of checking glass compositions with the inductively coupled plasma atomic emission spectroscopy, performed at PNNL, showed that no observable loss of volatile components (B, Li, Na, K, and Cs) occurred during glass preparation [7]. However, losses of  $\text{SO}_3$  and Cl do occur; these components were treated as “Others”.

Until recently, glasses prepared for testing were free of solids or phase separated liquids. The PNNL test procedure assures that any possible impact of volatility and crystallization that could occur during viscosity measurement on measured values would be detected. Measurement starts at 1150 °C, continues at higher temperatures up to 1250 °C, followed by taking data at lower temperatures up to 950 °C, typically at 50 °C steps, and finally returning to 1150 °C [2,7]. Thus, viscosity is measured twice for all but extreme temperatures and three times at 1150 °C. Viscosity deviations of repeated measurements would indicate effects of compositional nonuniformity (caused by volatilization) or phase inhomogeneity (caused by crystallization). These effects were generally absent because volatilization and crystallization do not occur or has no significant effect on data. For example, crystallization of spinels or separation of phosphates may occur in some extreme VSL compositions, but would not have any significant impact on

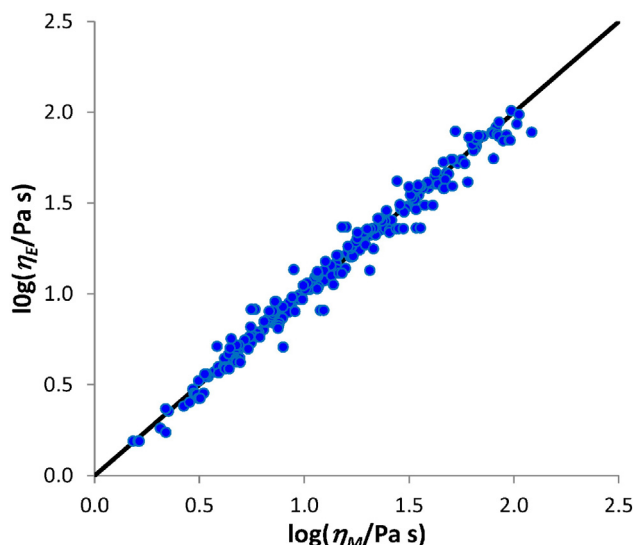


Fig. 4. Estimated versus measured values of  $\log \eta$  for the validation dataset.

viscosity values that model validation could reveal. It could affect component coefficients of the minor components involved, but this was avoided in the present study by treating those components as “Others”.

### 6. Component interactions

Larger databases with composition regions well covered with data points allow fitting of higher-order polynomials of the type

$$B = \sum_{i=1}^N B_i g_i + \sum_{i,j=1}^N B_{ij} g_i g_j + \sum_{i,j,k=1}^N B_{ijk} g_i g_j g_k \quad (5)$$

where  $B_{ij}$  and  $B_{ijk}$  are higher-order coefficients that represent binary and ternary interactions of components. The outlying data for VSL glasses that combine high fractions of both  $Al_2O_3$  and CaO suggest a possible interaction. However, the number of composition variations in the VSL dataset is not large enough for assessing higher-order terms.

### 7. Occam's razor

As stated in the Introduction, the main objective of this work is to determine the minimum number of parameters needed to represent the high-temperature viscosity as a function of temperature and melt composition. Such a task can be traced back to the famous Occam's razor, “Entities must not be multiplied beyond necessity.” This maxim can be applied to property–composition models as follows: *Among competing models that predict equally well, the one with the fewest adjustable coefficients (the parsimonious model) should be selected.*

The Arrhenius model, with a constant pre-exponential factor and a minimum possible  $B_i$  coefficients, performs satisfactorily for temperatures at which  $\log(\eta/Pa\ s) < 2.1$  for glasses with a relatively weak structure, such as nuclear waste glasses. Fig. 5 demonstrates that the common intercept of  $\log\eta$  versus  $T^{-1}$  lines (note that the intercepts is the high-temperature asymptote,  $\log \eta_\infty = -4.94$ , corresponding to  $A = \ln\eta_\infty = -11.38$ , see Table 2) provides an elegant and adequate representation for low-viscosity data. For stronger glasses, such as

commercial ones [14,18], the Arrhenius model is good for melts at temperatures at which  $\log(\eta/Pa\ s) < 3$ . Hence, there is no reason for fitting low-viscosity data with models possessing a number of parameters higher than  $N + 1$  except for higher-order coefficients justified by the effects of component interactions, as mentioned in Section 6.

Occam's razor is a requirement for simplicity and thus discourages overparameterization. In the case of glass melt viscosity, other negative aspects of overparameterization need to be considered. One is the loss of physical meaning of component coefficients. Additional coefficients do not inform us, or may even give us misleading information, about the role of individual components in the glass structure. Another aspect is faulty extrapolation, especially to extreme values of variables, which may be major model parameters, such as the high-temperature asymptote ( $\eta_\infty$ ), the viscosity at glass-transition temperature ( $T_g$ ), and the temperature at which viscosity rapidly increases to infinity ( $T_0$ ). Even though these extremes have no bearing on fitting data within a narrow interval of variables ( $T$  or  $\eta$ ), functions that do not lose meaning outside such intervals are clearly preferable. Concrete examples are given below to explore these aspects.

### 8. Approximation function with a higher number of composition-dependent parameters

*...it's all too easy to fit curves to data and convince yourself you've discovered some profound truth.*

[Robert Matthews]

#### 8.1. Arrhenius equation with composition-dependent A

The Arrhenius Eq. (1) is often fitted to low-viscosity data with two composition-dependent coefficients, A and B, i.e.,  $A = \sum A_i g_i$  and  $B = \sum B_i g_i$ , Eq. (2). Table 3 lists the component coefficients that result from performing such fitting for the VSL dataset (the other sets of coefficients listed in Table 3 are introduced in Sections 8.2 and 8.3). The coefficients

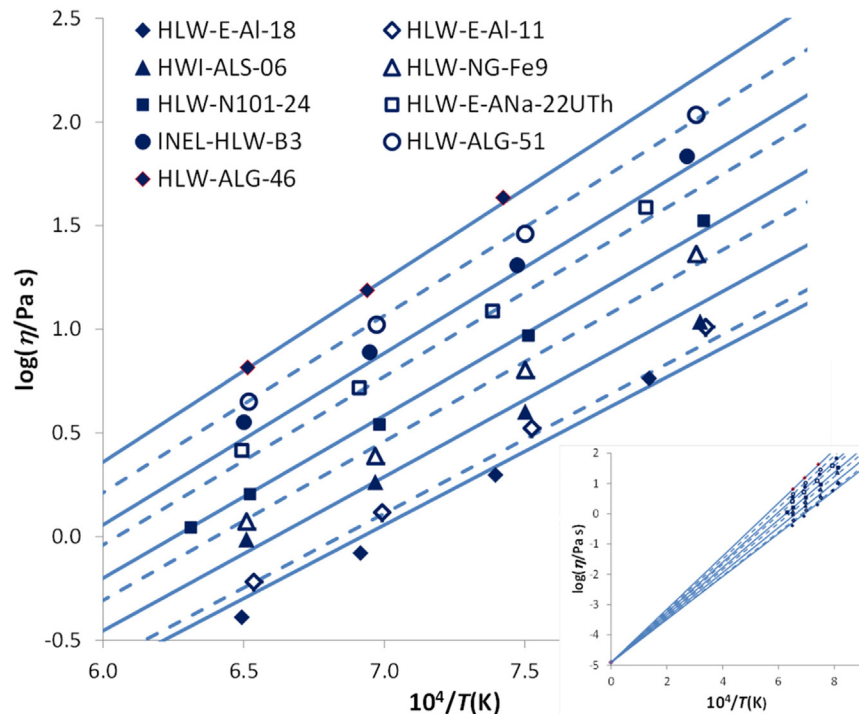


Fig. 5. Measured data and model estimates (the lines) for nine glasses from the HLW dataset (VSL glasses are identified as in [3]). The inset shows that all lines have a common intercept.

**Table 3**  
Component coefficients for the Arrhenius, VFT<sup>(a)</sup> (see Section 8.2), and Mauro et al. [24] (see Section 8.3) equations fitted to data and the maximum, minimum, and average values over the dataset.

	Arrhenius		VFT			Ref. [24]		
	$10^{-4}B_i$ (K)	$A_i$	$10^{-4}G_i$ (K)	$F_i$	$T_{0i}$ (K)	$10^{-4}K_i$ (K)	$J_i$	$L_i$ (K)
Al <sub>2</sub> O <sub>3</sub>	5.142	−24.1	3.145	−15.4	31	0.953	−5.9	1739
B <sub>2</sub> O <sub>3</sub>	0.045	−5.6	−0.583	−5.8	1074	−0.307	−4.9	2436
Bi <sub>2</sub> O <sub>3</sub>	0.116	−2.3	0.075	−1.9	359	−3.593	20.2	8916
CaO	1.025	−16.8	0.707	−15.8	327	−0.214	−10.6	1959
F	21.288	−166.8	11.876	−113.2	−962	39.739	−273.9	−81974
Fe <sub>2</sub> O <sub>3</sub>	3.196	−24.4	1.839	−16.3	−4	0.947	−13.6	258
K <sub>2</sub> O	−1.367	7.1	−1.401	9.5	664	−0.342	3.1	1195
Li <sub>2</sub> O	−11.187	37.4	−1.855	4.5	−2591	−0.635	−4.5	−4171
MgO	5.571	−39.9	11.947	−63.3	−4303	4.800	−35.9	−4255
MnO	−0.117	−4.6	2.348	−22.2	−549	1.518	−14.6	−2690
Na <sub>2</sub> O	−2.877	8.7	−1.764	6.3	288	−0.133	−1.9	−343
SiO <sub>2</sub>	3.220	−13.0	1.129	−4.7	771	0.264	−0.2	2286
SrO	3.912	−30.8	2.094	−19.4	−44	0.418	−12.9	1522
ZrO <sub>2</sub>	6.767	−41.5	5.619	−43.6	−112	3.407	−32.4	−1900
Others	2.583	−15.6	1.764	−13.4	154	0.423	−10.0	2229
Maximum <sup>(b)</sup>	2.699	−8.8	1.426	−5.4	538	0.674	−3.70	1528
Minimum <sup>(c)</sup>	1.314	−16.5	0.673	−11.2	219	0.265	−7.73	856
Average <sup>(d)</sup>	1.850	−11.4	0.954	−7.6	388	0.412	−5.18	1215

(a) VFT stands for Vogel-Fulcher-Tammann.

(b)–(d) Maximum, minimum, and average values for 395 data points.

were obtained by minimizing  $D_\eta$ , Eq. (3), using the expression of the right-hand side to include the component-dependent  $A$ . The maximum, minimum, and average values of the estimated  $A$  and  $B$  coefficients were computed for 395 individual data points.

The resulting decrease of the number of outliers (data for which  $D_\eta > 0.3$ ) from 5 to 1 and the increase of the  $R^2$  value to from 0.981 to 0.984 (Table 4) are miniscule improvements hardly worthy of the high number of parameters (30). The  $A_i$  coefficients, instead of being nearly equal for each component (which follows from the assertion that  $A = \text{constant}$  over the composition region), exhibit a large variability. Disregarding the unusual (and manifestly incorrect)  $A_i$  and  $B_i$  values for F, consistent with the high standard error of  $B_i$  (with  $A = \text{constant}$ ) in Table 2,  $A_i$  values range from  $−41.5$  (ZrO<sub>2</sub>) to  $37.4$  (Li<sub>2</sub>O). This result is grossly counterintuitive. It indicates that adding ZrO<sub>2</sub> would strongly decrease and Li<sub>2</sub>O strongly increase the asymptotic viscosity,  $\eta_\infty = e^A$ .

Variations in  $A_i$  values inevitably result in a large variation of  $A$ , from  $−16.5$  to  $−8.8$ , computed for individual data points. Based on both empirical data and theoretical reasoning,  $\eta_\infty \approx 10^{-5}$  Pa s [20,21,22,23]. This value corresponds to  $A = \ln(\eta_\infty) \approx −11.5$ , a virtually universal constant that only slightly changes with composition, but does not significantly change within a family of glasses, such as aluminoborosilicate nuclear waste glasses [18]. Values listed in Table 2 are close to this expected value, and so is the average in Table 3. The likely cause of the wide range of  $A$  values of individual glasses is experimental error. As Fig. 6 demonstrates, the deviations in  $A$  values are compensated by opposite deviations in  $B$  values. This compensation effect is a natural

**Table 4**  
Number of parameters ( $p$ ), number of outliers ( $\omega$ ), and correlation coefficients for various models.

Model	$p$	$\omega$	$R^2$	$R^2_{\text{adj}}$
Arrhenius equation with constant $A$	16	5	0.9811	0.9802
Arrhenius equation with composition-dependent $A$	30	1	0.9842	0.9829
VFT equation	45	1	0.9885	0.9869
VFT equation with constant $F$	31	1	0.9818	0.9802
VFT equation $T_g$ constrained	16	1	0.9804	0.9796
VFT equation double constrained	16	1	0.9628	0.9611
Mauro et al. equation	45	1	0.9907	0.9895
Mauro et al. equation with constant $J$	31	1	0.9867	0.9856
Mauro et al. equation $T_g$ constrained	15	1	0.9822	0.9815
Mauro et al. equation double constrained	15	1	0.9583	0.9565
Modified Adam-Gibbs equation	32	1	0.9792	0.9783
Modified Adam-Gibbs equation with $f = 7.837$	31	1	0.9790	0.9781

consequence of the large gap between measured data and the intercept as compared with the span of measured viscosities as the inset in Fig. 5 illustrates.

## 8.2. Vogel-Fulcher-Tammann equation

The Vogel-Fulcher-Tammann (VFT) equation,  $\ln \eta = F + G / (T - T_0)$ , has three temperature-independent parameters,  $F$ ,  $G$ , and  $T_0$ . It fits viscosity data within about 10 orders of magnitude of viscosity values, generally from  $10^3$  to  $10^{13}$  Pa s, in the temperature range at which glass structure rapidly changes. The VFT equation is suitable for applications such as glass forming or glass annealing. However, it fails for  $\eta < 10^2$  Pa s, when the melt is almost fully depolymerized and behaves like an ordinary liquid [19]. In spite of this known fact, this popular equation is habitually used for the low-viscosity range, where it is not adequate, and is fitted to low-viscosity data even when high-viscosity data, for which it has been designed, are not available.

Table 3 lists the component coefficients for the VFT equation with all three coefficients ( $F$ ,  $G$ , and  $T_0$ ) as composition-dependent first-order polynomials for 15 major glass components of the VSL dataset. The maximum, minimum, and average values of the estimated coefficient for each glass over the dataset sans the outlier are shown in the bottom rows of the table. The number of fitting parameters increased to 45. Again, the tiny gain in the  $R^2$  and  $R^2_{\text{adj}}$  values (Table 4) hardly justifies the large number of parameters.

By Giordano et al. [25],  $F = \text{constant}$ , independent of melt composition. Since  $\eta_\infty = e^F$ , the pre-exponential factors of the VFT and Arrhenius equations should be identical, i.e.,  $F = A$ . Yet for the VSL dataset (Table 3),  $F$  varied from  $−11.2$  to  $−5.4$  with an average value  $F = −7.6$ , far from the expected  $−11.5$ . Similar to  $A_i$  values and contrary to the expected behavior, the  $F_i$  values (Table 3) suggest that modifiers, such as Li<sub>2</sub>O, would increase the asymptotic viscosity and that glass formers, such as ZrO<sub>2</sub>, would decrease it. This impossible outcome is a consequence of the compensation effect, Fig. 6 [here  $B_{\text{VFT}} = d \ln \eta / dT^{-1} = G / (1 - T_0 / T)$ ]. Fitting the VFT equation to VSL data assuming a constant pre-exponential factor somewhat reduces overparameterization and results in a fair value of  $F = −11.48$ . However, the average  $T_0$  then becomes  $−7$  K, a nonphysical value.

Regarding  $T_0$ , it varies from 219 K to 538 K, with an average of 388 K, hardly reasonable values for temperatures at which glass turns into a brittle solid. It appears that the fitted coefficients  $F_i$  and  $T_{0i}$  mainly compensate for random errors and thus are a statistical fluke. The  $T_0$  value

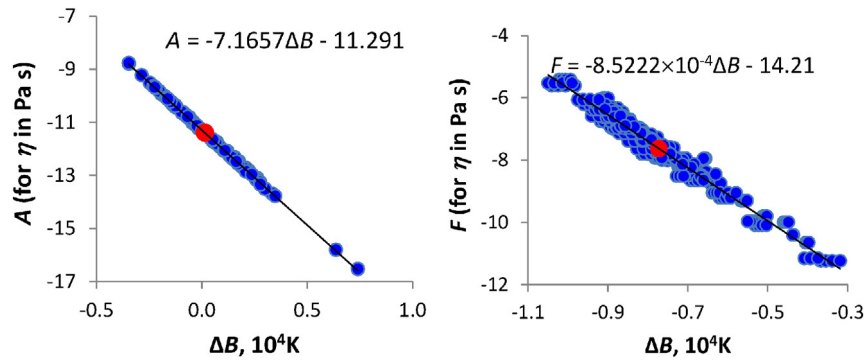


**Fig. 6.** Coefficient  $A = \Sigma A_{ig}$ , and coefficient  $F = \Sigma F_{ig}$ , versus activation energy difference for data fitted with the Arrhenius equation with both  $A$  and  $B$  composition dependent (left) and with the VFT equation with  $F$ ,  $G$ , and  $T_0$  composition dependent (right), each for 395 data points. Here  $\Delta B = B_{A(variable)} - B_{A(constant)}$  for the left plot and  $\Delta B = B_{VFT} - B_{A(constant)}$ , where  $B_{VFT} = G/(1 - T_0/T)$  for the right plot. The red points indicate average values. (For interpretation of the references to color in this figure legend, the reader is referred to the web version of this article.)

generally indicates the extent to which the structure of glass is changing. At high viscosities ( $\eta > 10^2$  Pa s),  $B$  in Eq. (1) changes with  $T$ . Assuming that  $A = F$  and comparing the VFT and Arrhenius equations, we get  $B(T) = G / (1 - T_0 / T)$ . Thus, the higher  $T_0$ , the greater the deviation from Arrhenius behavior (the weaker the melt). However, because the melt is Arrhenian at low viscosities, low-temperature data alone cannot be used to estimate the high-viscosity response.

Finally, as Fig. 7 shows, by the VFT equation, the activation energy,  $B = \partial \ln \eta / \partial T^{-1}$ , never becomes constant and decreases with the temperature even when viscosity is far below  $10^2$  Pa s. Because the glass structure no longer changes at low (measured) viscosities, there is no reason to anticipate that the structure would change when viscosities are still lower. The linear behavior shown in Fig. 5 is more likely.

### 8.3. Mauro et al. [24] equation

Another three-parameter equation,  $\ln \eta = J + (K/T) \exp(L/T)$ , was recently advanced by Mauro et al. [24]. Based on 568 Corning glasses,  $J$  narrowly varied around a single average value, which is in agreement with the near constancy of  $\eta_\infty = e^J$ . Table 3 lists the component coefficients of  $J$ ,  $K$ , and  $L$  obtained by fitting to VSL data. As Table 3 shows,  $J$  varied from  $-7.7$  to  $-3.7$  with the average value of  $J = -5.2$ , far

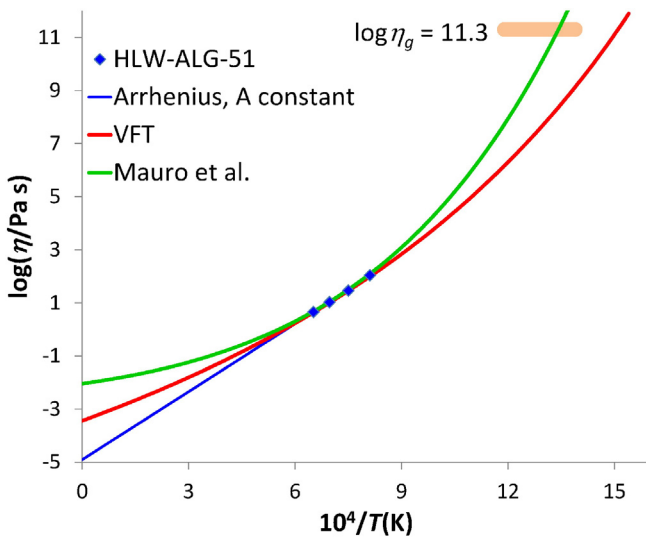


**Fig. 7.** Curves of  $\log \eta$  versus  $1/T$  from the high-temperature asymptote to glass transition for the VFT and Mauro et al. [24] equations based on coefficients listed in Table 3 and fitted to data from one of the VSL glasses (the VSL identification is shown in the legend). The Arrhenius function is not extrapolated to high viscosity because of its limited range of validity. The typical range of glass-transition temperatures is indicated by a bar at top right.

from the expected  $-11.5$ . As Fig. 7 indicates, the Mauro et al. [24]  $\log \eta$  versus  $T^{-1}$  function curves even more at low viscosities than the VFT function, which explains the high values of  $\eta_\infty$ . Regarding the  $J_i$  coefficients, their values exhibit anomalies similar to the  $F_i$  and  $A_i$  values. Unlike the VFT equation, the Mauro et al. [24] equation avoids a singularity at  $T > 0$ . Thus, whereas  $\eta \rightarrow \infty$  at  $T = T_0$  by the VFT equation,  $\eta \rightarrow \infty$  at  $T = 0$  by the Mauro et al. [24] equation. For the particular glass for which the curves are displayed in Fig. 7,  $\log \eta_{VFT}$  would shoot to infinity at  $T_0 = 329$  K, or  $10^4/T = 30$ . Fitting the Mauro et al. [24] equation to VSL data assuming a constant pre-exponential factor results in  $J = -7.64$ , a rather high value (as compared to  $A = -11.38$ ).

### 8.4. Constrained fits

Clearly, fitting VFT, Mauro et al. [24], or similar equations to low-viscosity data with a narrow span of values, such as those of the VSL dataset (0.4 to 242 Pa s), is unjustified. As argued above, it is objectionable even when data are available for high viscosities measured at lower temperatures because, by these equations, the activation energy,  $B = \partial \ln \eta / \partial T^{-1}$ , is changing with the temperature at low viscosities when the glass resembles an ordinary liquid. Yet such functions are used for modeling velocity fields in glass-melting furnaces where the viscosity is fairly well below  $10^2$  Pa s. Luckily, the errors caused by the lack of fit of the VFT and similar functions at high temperatures has been deemed acceptable for furnace modeling and the objectionable value of  $\eta_\infty$  has no bearing on the application.

It is a common practice to estimate the  $\log \eta$  versus  $T$  function over the whole technologically important interval from 1 to  $10^{12}$  Pa s by computing the values of three coefficients (such as  $F$ ,  $G$ , and  $T_0$ ) from three viscosity data sufficiently spread over the 10 to  $10^{12}$  Pa s interval. In fact, only two data points are needed for a glass of a known glass-transition temperature,  $T_g$ , assuming that  $\log(\eta_g/\text{Pa s}) \approx 12$ . By Nemilov [26], the  $\eta_g$  value depends on the cooling rate ( $\eta_g \approx 10^{12.8}$  Pa s at  $-3$  K/min) and is lower for weak glasses with low shear moduli (for organic glasses,  $\eta_g$  can be as low as  $10^{10}$  Pa s).

For nuclear waste glasses, the measured values of  $T_g$  range from 720 to 840 K and  $\log(\eta_g/\text{Pa s}) = 11.3$  [18]. This interval is indicated in Fig. 7, which shows the extrapolated VFT and Mauro et al. [24]  $\log \eta$  versus  $1/T$  functions from the high-temperature asymptote to glass transition for one of the VSL glasses with the identification shown in the legend; the lines were computed using the component coefficients listed in Table 3. As argued above, extrapolating the VFT equation fitted to low-viscosity data to high viscosities is unsound, yielding a flawed  $T_0$  value. It is no wonder that, as Fig. 7 illustrates, the VFT function misses the experimental  $T_g$  range, greatly underestimating  $T_g$ . For the VSL dataset, the extrapolated VFT equation yields  $T_g$  values within a range of 400 to 990 K (670 K average) that is much broader than the experimental range. The Mauro et al. [24] equation does not perform

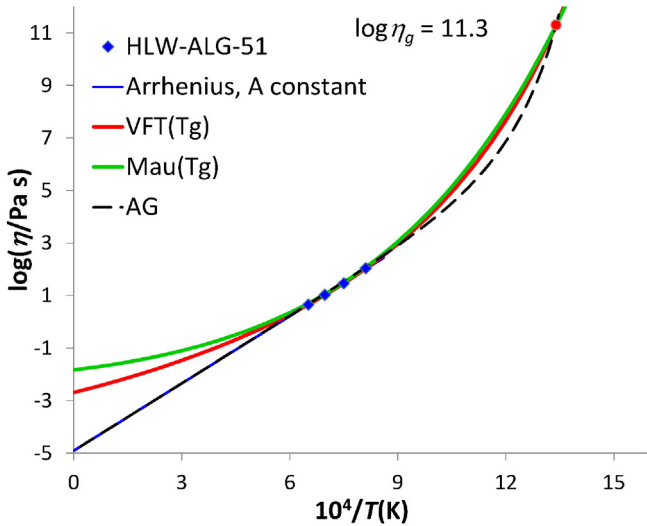


**Fig. 8.** Curves of  $\log \eta$  versus  $1/T$  from the high-temperature asymptote to glass transition for the VFT and Mauro et al. [24] equations fitted to VSL data and constrained to  $\log(\eta_g/\text{Pa s}) = 11.3$  at  $T_g = 746$  K. The curve based on the modified Adam-Gibbs function (AG) is also displayed.

much better, anticipating for VSL glasses the range of  $T_g$  values from 470 to 1020 K (720 K average), even though it appears luckier for the composition selected for demonstration in Fig. 7, where it reasonably approximates the low-temperature behavior.

As indicated above, if the  $T_g$  value is known, or can be reliably estimated, one can use the  $\eta_g$  value, which is independent of composition, to constrain the three-coefficient equations and obtain a rough estimate of the whole  $\log \eta$  versus  $T^{-1}$  curve based on just two additional viscosity data. Fig. 8 shows the result of such fitting for one VSL glass for which the  $T_g$  was estimated based on coefficients reported in [18]. The  $\eta$  versus  $T$  relationship is probably unreliable for high viscosities ( $>10^2$  Pa s) because of the lack of any data between  $10^2$  and  $10^{11}$  Pa s and also because the  $T_g$  model used was based on a composition region smaller than that of the VSL dataset. With the  $T_g$  constrained fitting, the lines in Fig. 8 are

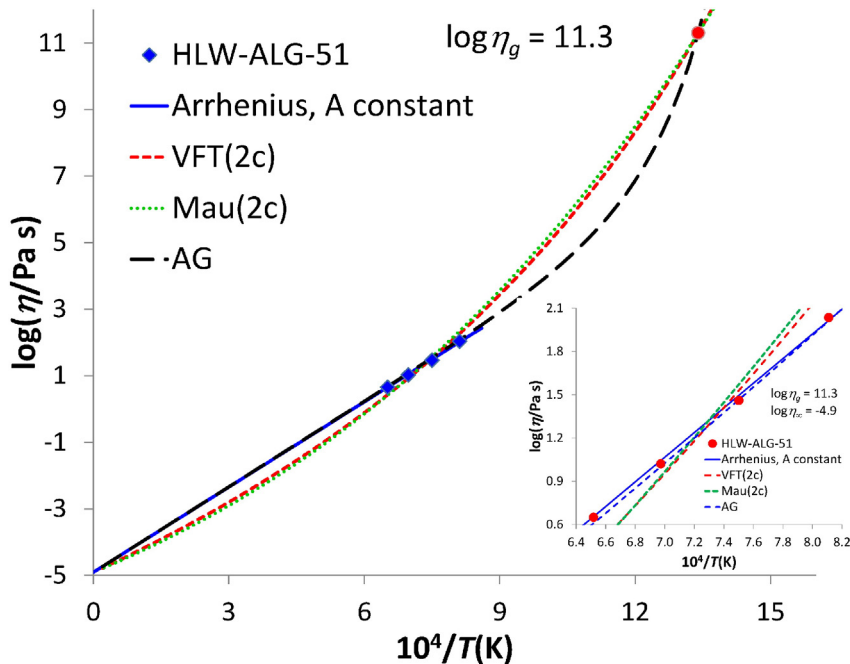


**Fig. 9.** Curves of  $\log \eta$  versus  $1/T$  from the high-temperature asymptote to glass transition for the VFT and Mauro et al. equations fitted to VSL data and constrained to  $\log(\eta_g/\text{Pa s}) = 11.3$  at  $T_g = 746$  K and to  $\log(\eta_\infty/\text{Pa s}) = -4.9$  at  $T \rightarrow \infty$ . The curve based on the modified Adam-Gibbs function is also displayed.

curved at low viscosities even more than in Fig. 7, where no constraining was imposed.

It is obvious that nothing can be done to improve the fit of the VFT and Mauro et al. [24] equations to low-viscosity data. Double-constrained equations for which both  $\eta_g$  and  $\eta_\infty$  have predetermined values independent of composition require only a single data point for assessing three coefficients. Fig. 9 shows the result for the selected VSL glass. The lines curve at high temperatures to the extent that, as the inset demonstrates, the functions exhibit a significant lack of fit for low-viscosity data.

Table 4 compares the correlation coefficients of several model variations fitted to the VSL dataset. The table demonstrates that the increased  $R^2$  values and decreased numbers of outliers (data for which  $[\ln(\eta_M/\eta_E)]^2 > 0.3$ ) brought miniscule improvements of the fit of the increased number of parameters. Moreover, as shown above, these tiny improvements are at the expense of the sound physics.

### 8.5. Modified Adam-Gibbs equation

A modified Adam-Gibbs equation can be written in the form  $Y = (T_g/T)[s_0 - (s_0 - 1)(T_g/T)^f]^{-1}$ , where  $Y = \ln(\eta/\eta_\infty) / \ln(\eta_g/\eta_\infty)$  is normalized  $\ln \eta$ ,  $s_0 = \sum s_{0i} g_i$  is the dimensionless configurational entropy at  $T \rightarrow \infty$ , and  $f$  is an exponent related to glass fragility [18]. For HLW glasses,  $f$  ranges from 7 to 8; the VFT equation is a special case of  $f = 1$  [18].

The modified Adam-Gibbs equation was fitted to the VSL dataset with  $T_g$  values estimated using coefficients from previous work [18]. Component coefficients for  $s_0$  are listed in Table 5. The value of  $f = 7.511$  was obtained using the least squares method, minimizing  $D_\eta$ , the expression of the right-hand side of Eq. (3). The number of parameters is  $2N + 2 = 32$  ( $N$  parameters for  $s_0$  and for  $T_g$ , one for  $\eta_\infty$ , and one for  $f$ ). This is a minimum number of fitting parameters needed for the full range of viscosity including the low values. As Fig. 9 shows, the activation energy is virtually constant for  $\eta < 10^2$  Pa s. Because high-viscosity data are unavailable, the section of the curve above  $10^2$  Pa s cannot be verified. The equation was also fitted with a predetermined  $f = 7.837$  taken from [18]. The lower number of fitting parameters (31) resulted in a slightly lower  $R^2$  (Table 4).

**Table 5**  
Component coefficients  $s_{oi}$  for the modified Adam–Gibbs equation.

	$s_{oi}$
Al <sub>2</sub> O <sub>3</sub>	0.250
B <sub>2</sub> O <sub>3</sub>	2.739
Bi <sub>2</sub> O <sub>3</sub>	1.736
CaO	3.239
F	2.280
Fe <sub>2</sub> O <sub>3</sub>	1.809
K <sub>2</sub> O	1.800
Li <sub>2</sub> O	4.735
MgO	1.821
MnO	2.086
Na <sub>2</sub> O	2.411
SiO <sub>2</sub>	0.878
SrO	1.765
ZrO <sub>2</sub>	1.303
Others	1.055

Although  $T_0$  is an extrapolated asymptote at which  $\eta \rightarrow \infty$ , its value is entirely hypothetical and even paradoxical (Kauzman paradox). Its value depends on the form of the approximation function. By the modified Adam–Gibbs equation,  $T_0 = T_g[s_0/(1 - s_0)]^{1/f}$  the value of which is spanning the range of 300 to 420 K with an average of 350 K for the VSL dataset. The actual value can hardly be experimentally verified and is as good as  $T_0 = 0$ , a value proposed by Mauro et al. [24] and others before them. Nevertheless, not far below  $T_g$ , glass behaves as a brittle solid for all practical purposes.

## 9. Conclusion

The Arrhenius equation with a constant pre-exponential factor and the activation energy a function of composition in terms of mass or mole fractions of influential components is sufficient to represent the viscosity of high-level nuclear waste glasses with  $\eta$  up to 240 Pa s. Increasing the number of parameters either by assuming that the Arrhenius pre-exponential factor is a function of composition, or that the VFT equation coefficients are composition dependent, does not bring any significant improvement of the fit and results in physically meaningless values of component coefficients. The Arrhenius equation is a high-temperature approximation of a modified Adam–Gibbs equation that represents the full range of viscosity of glasses from  $\eta_\infty \approx 10^{-5}$  Pa s to  $\eta_g \approx 10^{12}$  Pa s.

## Acknowledgments

This work would not been done without inspiration by Mary Nelson, a student curious about application of statistical methods to waste glass development. We are grateful to John Vienna for making the VSL dataset available to us in an electronic form. We would also like to express our deep gratitude to our colleagues Mike Schweiger, Dong-Sang Kim, Jaehun Chun, Matt Chou, Tony Jin, and many others for their interest and helpful discussions. Special thanks to Scott Cooley for his many comments and suggestions. Finally, many thanks to Jarrod Crum, who thoroughly evaluated the dataset with scatterplots and histograms, so we could continue our work with greater confidence. The This work was managed by Albert A. Kruger with funding authorized by the Federal Project Director William F. Hamel, Jr. of the U.S. Department of Energy's Waste Treatment and Immobilization Plant (Work Order MOORV00020). Pacific Northwest National Laboratory (PNNL) is

operated for the DOE by Battelle Memorial Institute under contract DE-AC05-76RL01830.

## References

- [1] P. Hrma, S.-S. Han, Viscosity of glasses for radioactive waste, *J. Non-Cryst. Solids* 358 (2012) 1818–1829.
- [2] P. Hrma, B.M. Arrigoni, M.J. Schweiger, Viscosity of many-component glasses, *J. Non-Cryst. Solids* 355 (2009) 891–902.
- [3] I.S. Muller, W.K. Kot, H.K. Pasioka, K. Gilbo, F.C. Perez-Cardenas, I. Joseph, I.L. Pegg, *Compilation and Management of ORP Glass Formulation Database*, VSL-12R2470-1, ORP-53934, Vitreous State Laboratory, Catholic University of America, Washington, D.C., 2012 (<http://www.osti.gov/scitech/biblio/1059497-compilation-management-orp-glass-formulation-database-vsl-rev>).
- [4] H. Scholze, *Glass*, Springer, New York, 1990 172.
- [5] M. Zimova, S.L. Webb, The combined effect of chlorine and fluorine on viscosity of aluminosilicate melts, *Geochim. Cosmochim. Acta* 71 (2007) 1553–1562.
- [6] J.D. Vienna, A. Fluegel, D.S. Kim, P. Hrma, *Glass Property Data and Models for Estimating High-Level Waste Glass Volume*, PNNL-18501, Pacific Northwest National Laboratory, Richland, Washington, 2009.
- [7] P. Hrma, G.F. Piepel, M.J. Schweiger, D.E. Smith, D.-S. Kim, P.E. Redgate, J.D. Vienna, C.A. LoPresti, D.B. Simpson, D.K. Peeler, M.H. Langowski, *Property/Composition Relationships for Hanford High-Level Waste Glasses Melting at 1150 °C*, PNL-10359, vol. 1 and 2 Pacific Northwest Laboratory, Richland, Washington, 1994.
- [8] P. Hrma, G.F. Piepel, P.E. Redgate, D.E. Smith, M.J. Schweiger, J.D. Vienna, D.-S. Kim, Prediction of processing properties for nuclear waste glasses, *Ceram. Trans.* 61 (1995) 505–513.
- [9] J.D. Vienna, P. Hrma, D.-S. Kim, M.J. Schweiger, D.E. Smith, Compositional dependence of viscosity, electrical conductivity, and liquidus temperature of multicomponent borosilicate glasses, *Ceram. Trans.* 72 (1996) 427–436.
- [10] G.F. Piepel, A. Heredia-Langner, S.K. Cooley, Property–composition–temperature modeling of waste glass melt data subject to a randomization restriction, *J. Am. Ceram. Soc.* 91 (2008) 3222–3228.
- [11] S.K. Cooley, G.F. Piepel, H. Gan, W.K. Kot, I.L. Pegg, A two-stage layered mixture experiment design for a nuclear waste glass application (parts 1 and 2), 2003 Proceedings of the American Statistical Association, American Statistical Association, Alexandria, VA 2003, pp. 1036–1051.
- [12] G.F. Piepel, S.K. Cooley, J.D. Vienna, J.V. Crum, Experimental Design for the Initial Phase of the Hanford low-Activity Waste Enhanced Glass Study, PNNL-24391, Rev. 1, Pacific Northwest National Laboratory, Richland, WA, 2015 ([http://www.pnl.gov/main/publications/external/technical\\_reports/PNNL-24391.pdf](http://www.pnl.gov/main/publications/external/technical_reports/PNNL-24391.pdf)).
- [13] A.L. Kieplinski Sadler, A new viscosity model for waste glass formulations, *Ceram. Trans.* 72 (1996) 85–92.
- [14] P. Hrma, High-temperature viscosity of commercial glasses, *Ceramics Silikaty* 50 (2006) 57–66.
- [15] A. Fluegel, Glass viscosity calculation based on global statistical modeling approach, *Eur. J. Glass Sci. Technol. A* 48 (2007) 13–30.
- [16] M.I. Ojovan, K.P. Travis, R.J. Hand, Thermodynamic parameters of bonds in glassy materials from viscosity–temperature relationships, *J. Phys. Condens. Matter* 19 (2007) 415107.
- [17] M.I. Ojovan, Viscous flow and the viscosity of melts and glasses, *Eur. J. Glass Sci. Technol. B* 53 (2012) 143–150.
- [18] P. Hrma, Glass viscosity as a function of temperature and composition: a model based on Adam–Gibbs equation, *J. Non-Cryst. Solids* 354 (2008) 3389–3399.
- [19] D.R. Neuville, Viscosity, structure and mixing in (Ca, Na) silicate melts, *Chem. Geol.* 229 (2006) 28–41.
- [20] S. Glasstone, K.J. Laidler, H. Eyring, *The Theory of Rate Processes: The Kinetics of Chemical Reactions, Viscosity, Diffusion and Electrochemical Phenomena*, McGraw-Hill, New York, 1941.
- [21] C.A. Angel, Structural instability and relaxation in liquid and glassy phases near the fragile liquid limit, *J. Non-Cryst. Solids* 102 (1988) 205–221.
- [22] J. Russell, D. Giordano, A model for silicate melt viscosity in the system CaMgSi2O5–CaAl2Si2O8–NaAlSi3O8, *Geochim. Cosmochim. Acta* 69 (2005) 5333–5349.
- [23] M.L.F. Nascimento, C. Aparico, Data classification with the Vogel–Fulcher–Tammann–Hesse viscosity equation using correspondence analysis, *Physica B* 398 (2007) 71–77.
- [24] J.C. Mauro, Y. Yue, A.J. Ellison, P.K. Gupta, D.C. Allan, Viscosity of glass-forming liquids, *Proc. Natl. Acad. Sci. U. S. A.* 106 (2009) 19780–19784.
- [25] D. Giordano, A. Mangiacapra, M. Potuzak, J.K. Russell, C. Romano, D.B. Dingwell, A. Di Muro, An expanded non-Arrhenian model for silicate melt viscosity: a treatment for metaluminous, peraluminous, and peralkaline liquids, *Chem. Geol.* 229 (2006) 42–56.
- [26] S.V. Némilov, Maxwell equation and classical theories of glass transition as a basis for direct calculation of viscosity at glass transition temperature, *Glas. Phys. Chem.* 39 (2013) 609–623.